CONFIDENCE ESTIMATION IN IVUS RADIO-FREQUENCY DATA WITH RANDOM WALKS

Athanasios Karamalis[⋆] *Amin Katouzian*[⋆] *Stephane Carlier*[†] *Nassir Navab*[⋆]

[⋆] Computer Aided Medical Procedures (CAMP), Technische Universität München, Germany
[†] Universitair Ziekenhuis Brussel, Department of Cardiology, Belgium

ABSTRACT

The shadow regions in ultrasound (US) B-mode images are due to severe reflection of backscattered signals from dense tissue/medium interface. The loss of ultrasound energy as well as lack of textural or spectral features in these regions raise uncertainty, resulting confusion among experts decisions and developed computer-aided diagnosis (CAD) algorithms outcomes. In this paper, we present a novel uncertainty (confidence) estimation method, modeling the problem through random walk under particular constrains motivated by underlying physics of ultrasound. We demonstrate that constructed confidence maps can then be employed in different ultrasound based CAD algorithms, which ultimately improve experts qualitative and quantitative assessments. We evaluate our method on intravascular ultrasound (IVUS) radiofrequency (RF) data and quantify the results through non-linearly registered histology image as ground-truth.

Index Terms— IVUS, RF, Confidence, Random Walks, Graph Laplacian

1. INTRODUCTION

The IVUS is an imaging modality that provides cross-sectional images of arterial wall and extend of atherosclerosis disease in real-time. The IVUS grayscale images alone or combined with processing of backscattered RF signals can be employed for further characterization of plaques and more importantly identification of vulnerable ones [1]. As a result, several atherosclerotic tissue classification (TC) algorithms such as virtual histology (VH) [2] have been developed to assist interventional cardiologists to better characterize plaque constitutes and delineate rupture-prone ones. However, the main limitation of VH algorithm is that it systematically classifies tissues in hypoechoic regions behind arc of calcified plaques [3] where loss of acoustic energy is expected. Similar arguments are also valid for shadowing regions due to tissue-lung interface, where relatively strong signals are recorded but mainly ignored by experts and marked as unreliable information. Moreover, from segmentation perspective, the shadow artifact makes regularization very challenging. For example, a guide-wire close to surface of IVUS transducer element or appearance of side-branch often require special care to provide the final automated detected lumen border in closed smooth elliptical form.

These have motivated researchers to come up with a quantitative index such as confidence map for measuring uncertainty in the US grayscale or RF signals and alleviate inter- as well as intra-observer variability in diagnosis procedures. The classical approach is to construct a special map of attenuation coefficients associated with tissues [4] and assign low confidence labels to those that represent high attenuation and vise versa. Despite significant improvements, accurate and robust estimation of attenuation coefficients still remains an illusive goal [5]. Integrating intensities along scan-lines of US has also been a simple and commonly applied approach in medical image computing algorithms like segmentation and registration for detecting shadow regions [6] that improves the overall results of CAD algorithms, however, it is highly dependent on local characteristics of grayscale images and often requires for empirically selected thresholds.

We establish our confidence estimator upon novel formulation of US transmission, beam-width, and depth dependent attenuation through random walk framework. In particular, we adapt an analytical solution, provided by Grady [7], where the random walk problem is modeled by discrete equilibrium equations [8]. The main advantage of our proposed technique is that it can be applied on both grayscale images and RF signals.

2. METHODS

We formulate the estimation of the confidence maps and adopt a modified version of analytic solution to the random walk problem introduced by Grady [7]. To better present the modifications, we begin with a brief description of the original random walks for image segmentation algorithms [7].

2.1. Random Walks for Image Segmentation

In this method, user places seeds/labels in regions for multi-label segmentation. The target image or volume is handled as a discrete object by representing pixels as nodes $v \in V$ that are connected by weighted w_{ij} edges $e_{ij} \in E$; forming

This work was partly funded by the European project "PASSPORT" Grant Agreement no: 223894.

a graph Laplacian $G = (V, E)$. Subsequently, the probability of a random walk, reaching one of the label nodes first, is computed for every unlabeled node in the graph. The analytic solution to the desired probabilities is derived from the Laplacian matrix

$$L_{ij} = \begin{cases} d_i & \text{if } i = j \\ -w_{ij} & \text{if } v_i \text{ and } v_j \text{ adjacent nodes} \\ 0 & \text{otherwise} \end{cases} \quad (1)$$

where $d_i = \sum_j w_{ij}$ and w_{ij} is the weight connecting two nodes v_i and v_j. In the original work, a Gaussian weighting function was chosen $w_{ij} = \exp(-\beta(g_i - g_j)^2)$, where g_i was pixel intensity at node i and β was a free parameter, which was set to a constant value for all experiments in the original and our own framework ($\beta = 90$). To obtain the solution and to practically apply necessary boundary conditions imposed by labeled nodes, L is re-ordered and decomposed into blocks of marked M and unmarked nodes U:

$$L = \begin{bmatrix} L_M & B \\ B^T & L_U \end{bmatrix} \quad (2)$$

The desired probabilities are obtained by solving $L_U x_U = -B^T x_M$ where x_U and x_M are known and unknown probabilities at seed nodes, respectively.

2.2. Estimation of Confidence Through Random Walks

To begin with, we shall compute the probability associated with a random walk, starting at an arbitrary node, that reaches one of the virtual transducer elements first. In general, these elements are modeled by initializing seeds at the nodes corresponding to the beginning of each US scan-line. The seeds are also placed at the end of each scanline to satisfy boundary conditions when solving for L. This effectively incorporates absorption region after which no signal is received/recorded. A schematic of seed positioning is shown in Figure 1. The graph representation encompasses arbitrary topologies, which effectively allows for modeling any transducer geometry. In our application, we derive the confidence maps directly from RF data collected in polar coordinate that is the original domain of acquisition. Therefore, a regular and equidistant lattice representation suits our modeling the best. In the classical random walk problem for segmentation applications, the desirable solution is a 'cut' through globally strongest gradients. However, we need to adapt the random walk behavior with US specific constrains in order to compute confidence or uncertainty in the data acquired with US. Hence, we define a new weighting function to adjust the behavior as:

$$w_{ij} = \begin{cases} w_{ij}^H & \text{if } i,j \text{ adjacent and } e_{ij} \in E_H \\ w_{ij}^D & \text{if } i,j \text{ adjacent and } e_{ij} \in E_D \\ w_{ij}^V & \text{if } i,j \text{ adjacent and } e_{ij} \in E_V \\ 0 & \text{otherwise} \end{cases} \quad (3)$$

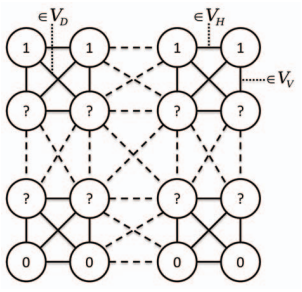


Fig. 1. Illustration of the 8-connected Laplacian graph and automatic seed placement.

$$w_{ij}^H = \exp(-\beta((c_i - c_j)^2 + \gamma)) \quad (4)$$

$$w_{ij}^D = \exp(-\beta((c_i - c_j)^2 + \sqrt{2} \cdot \gamma)) \quad (5)$$

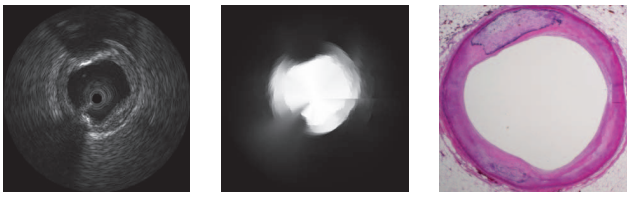
$$w_{ij}^V = \exp(-\beta((c_i - c_j)^2)) \quad (6)$$

where E_H, E_D, E_V are edges along horizontal, diagonal, and vertical graph directions, respectively (Fig. 1), $E_H \ominus E_D \ominus E_V = E$, $c_i = |r_i| \exp(-\alpha x_i)$, r_i is the absolute RF signal, and x_i is the normalized closest distance from node v_i to the virtual transducer elements (seeds).

To better appreciate the newly defined weighting function, one may think of the random walks as a circuit problem in potential theory, as discussed in [7, 8]. In order to correctly justify the correlation between confidence values and acoustic energy, we must take into account the inverse proportionality of reflected and transmitted signals energies, i.e., the stronger the reflection the weaker the transmission at tissue/medium interface and vice versa [9]. This is represented by the gradient term $c_i - c_j$ that expresses such behavior while the overall potential/probability for a node decreases with increasing weights/resistance along the random walk path. Notice that the change of signal amplitude r_i was also reflected as absolute RF signal in c_i.

In US image acquisition, transmitted signal is focused within a narrow-beam along each scanline and anything outside the beam-width does not contribute notably to the image formation. Consequently, the beam-width needs to be modeled into the random walks behavior. This is realized with the additive γ parameter, which effectively penalizes diagonal and horizontal walks away from the scanline where the walk is initiated from. As we can see, the probability of diagonal and horizontal walks is inversely proportional to the distance. Diagonal walks are penalized more due to their longer relative distances by factor of $\sqrt{2}$. Interpreted in circuit theory, the γ parameter increases overall resistance of a path as horizontal/diagonal distance to its origin is increased.

Finally, one of the fundamental properties of US is the attenuation of the US signal energy as it originates from transducer and travels. Different models have been proposed for depth dependent attenuation [9], including the Beer-Lambert law, which we adopt to our framework in the c_i function,



(a) B-Mode (b) Confidence Map (c) Histology

Fig. 2. Example from our evaluation dataset showing: (a) IVUS B-Mode, (b) corresponding confidence map, and (c) the corresponding histology.

resulting in low confidence values as distance x_i increases. Combined with the absolute RF amplitude r_i the function expresses depth dependent attenuation, which is still dependent on the image content. For example, strong echoes close to transducer elements shall introduce low confidence values.

3. EXPERIMENTS AND RESULTS

In our experiments, the IVUS RF data was acquired from dissected coronary arteries from autopsied hearts 24 hours postmortem. The experiment setup and acquisition protocol are presented in [10]. We performed our algorithm on raw IVUS RF signals, prior to log compression and normalization, estimated confidence, and constructed corresponding maps. Finally, we quantified results using corresponding histology images. An example of the qualitative evaluation is given in Figure 2. In the confidence map, a bright gray levels indicates high confidence and vice versa. Comparing the map to the B-mode image, we clearly observe a drop of confidence at the IVUS guide-wire, the media-adventitia (MA) border due to hypoechoic property of smooth muscle cells, and at highly reflective interfaces that cause shadowing. Looking at the corresponding histology it becomes clear that these interfaces are at the border of some tissues with especial interest such as calcification and necrotic core that are known factors associated with vulnerable plaques. These regions usually appear as dark areas in IVUS images due to rapid attenuation of signals. The constructed confidence map from RF signals clearly demonstrates that there is not much information and confirms unreliability of tissue characterization results in corresponding regions.

We quantified our results by manually labeling necrosis/calcified and fibrotic/lipidic regions where severe attenuation of ultrasound signals is expected in the former case but not latter, resulting low (LC) and high confidence (HC) values, respectively. In order to obtain the most accurate and reliable results, the labeling was performed on histology images, where pathological structures were easily distinguishable by histopathologist, and then transformed onto corresponding IVUS image and confidence map through non-linear registration technique. Figure 3 illustrates the

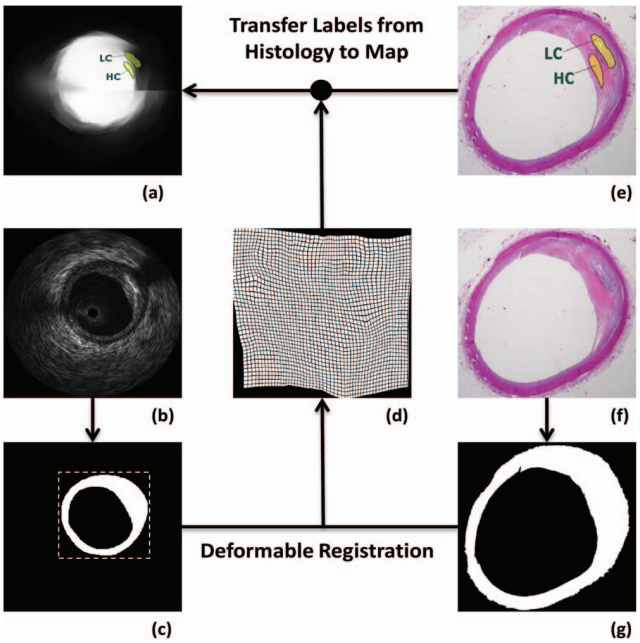


Fig. 3. Illustration of the deformable registration pipeline for mapping labels assigned in histology to confidence maps. Image details: (a) labeled confidence map, (b) IVUS, (c) segmentation mask (dotted-box is the bounding-box for size-normalization), (d) deformation field, (e) labeled histology, (f) histology, and (g) segmentation mask.

process and resulting images. This was in fact one of the advantageous of designed experimental setup and acquisition protocol described in [10] that ensured reliable IVUS-histology matching procedure. Nevertheless, the deformation of inner wall due to formalin fixation that was used prior to histology preparation demanded for a deformable model registration between IVUS and corresponding histology image in order to find one-to-one labels correspondences. In brief, an intermediate representation of images, which in our case are size-normalized segmentation masks from both IVUS and histology were obtained automatically for the IVUS images and semi-automatically from the histology images using random walks segmentation [7]. Subsequently, deformable registration is computed between the segmentation masks, using the Markov Random Field (MRF) registration framework introduced in [11][1]. The availability of different penalty functions for regularization of the deformation field was decisive for this choice, given additional constrains that needed to be imposed because of missing image information using only binary masks. Finally, the resulting deformation field was utilized to map the HC and LC labels from the histology to the corresponding confidence maps. With this experimental setup the confidence maps could be sampled at HC and LC defined in co-registered histology images as depicted in

[1]Framework can be downloaded at http://www.mrf-registration.net/

Figure 3. This entire process was repeated for a total of 13 IVUS images and associated labels. The statistics of these sampled regions are presented in Figure 4. The results indicate a good separation between HC and LC regions, which is highly desirable for regularizing in segmentation algorithms and more importantly evaluation of presence of informative regions in regions behind arc of calcified plaques, which has always been a controversial subject in tissue characterization. Our quantitative results confirm that there is not sufficient acoustic information and therefore particular attention must be paid when interpreting tissues in these regions. It is also evident that the confidence values are not distinct for same areas in different dataset. This is expected given that sound travels through different mediums with different acoustic impedances to reach the HC and LC region in the different datasets. Essentially, the path to these regions involves different energy reduction for each dataset. Although the registration was affirmative, it introduced minor errors due to severe deformation of inner wall in histology images. Consequently, the standard deviation of some sample regions varied proportional to extend of deformation.

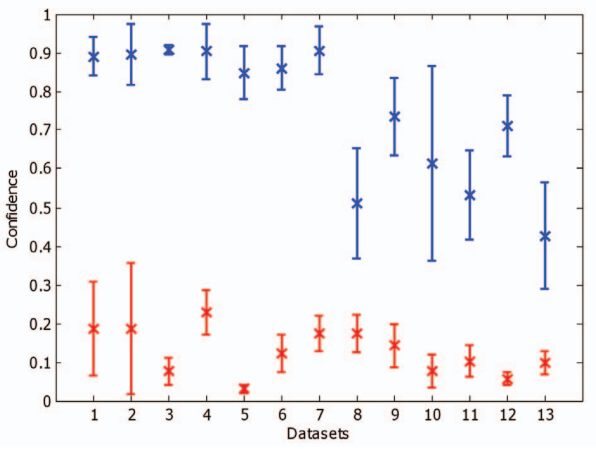


Fig. 4. Sampling of confidence maps at HC (blue) and LC (red) regions defined in co-registered histology. Each bar shows the mean and and the (+/-) standard deviation of the confidence sampled in the labeled regions.

4. CONCLUSION

We presented a novel method to model transmission/reflection of ultrasound signals by incorporating ultrasound-specific constrains into random walks framework and constructed confidence maps. For the first time, we registered IVUS and histology images and illustrated the outcomes. All these, enabled us to search for the most representative regions in ultrasound images or flagged out those that did not carry any informative features. We evaluated our algorithm performance, deploying IVUS RF signals and demonstrated encouraging results. Our results confirmed lack of acoustic energies in regions behind arc of calcified plaques or those with late necrosis. In general, constructed confidence maps could result in reducing inter- and intra-variability of experts diagnosis decisions particularly in regions that are challenging to interpret due to uncertainty in presence of information. In future, we will use constructed confidence maps to detect guide-wire as well as side-branches regularization of border detection results in segmentation algorithms.

5. REFERENCES

[1] G. W. Stone and Maehera et al, "A prospective natural-history study of coronary atherosclerosis," *New Eng. J. Med.*, vol. 364, pp. 226–235, 2011.

[2] A. Nair, B. D. Kuban, and M. et al Tuzcu, "Coronary plaque classification with intravascular ultrasound radiofrequency data analysis," *Circulation*, vol. 106, no. 17, pp. 2200–2206, 2002.

[3] G. S. Mintz and E. Missel, "What is behind the calcium? The relationship between calcium and necrotic core on virtul histology analyses:reply," *Letters to the Editor, European Heart Journal*, vol. 30, pp. 125–126, 2009.

[4] R. Kuc and H. Li, "Reduced-order autoregressive modelling for center-frequency estimation," *Ultrasonic Imaging*, vol. 7, pp. 244–251, 1995.

[5] JA Noble, "Ultrasound image segmentation and tissue characterization," *Proceedings of the Institution of Mechanical Engineers, Part H: Journal of Engineering in Medicine*, vol. 224, no. 2, pp. 307, 2010.

[6] Wolfgang Wein, Barbara Röper, and Nassir Navab, "Integrating diagnostic B-mode ultrasonography into CT-based radiation treatment planning," *IEEE TMI*, vol. 26, pp. 866–879, 2007.

[7] L. Grady, "Random walks for image segmentation," *IEEE TPAMI*, vol. 28, pp. 1768–1783, 2006.

[8] G. Strang, "A framework for equilibrium equations," *SIAM Review*, vol. 30, pp. 283–297, 1988.

[9] Richard S. C. Cobbold, *Foundations of Biomedical Ultrasound*, Oxford University Press, 2006.

[10] Amin Katouzian and Andrew F. Laine, *Methods in Atherosclerotic Plaque Characterization Using Intravascular Ultrasound (IVUS) Images and Backscattered Signals*, Springer, 2010.

[11] B. Glocker, N. Komodakis, G. Tziritas, N. Navab, and N. Paragios, "Dense image registration through mrfs and efficient linear programming," *Medical Image Analysis*, vol. 12, no. 6, pp. 731–741, 2008.